Accepted Manuscript

Hierarchical structured and programmed vehicles deliver drugs locally to inflamed sites of intestine

Wei Li, Yunzhan Li, Zehua Liu, Nattha Kerdsakundee, Ming Zhang, Feng Zhang, Xueyan Liu, Tomás Bauleth-Ramos, Wenhua Lian, Ermei Mäkilä, Marianna Kemell, Yaping Ding, Bruno Sarmento, Ruedeekorn Wiwattanapatapee, Jarno Salonen, Hongbo Zhang, Jouni T. Hirvonen, Dongfei Liu, Xianming Deng, Hélder A. Santos

PII: S0142-9612(18)30661-6

DOI: 10.1016/j.biomaterials.2018.09.024

Reference: JBMT 18895

To appear in: *Biomaterials*

Received Date: 12 August 2018

Revised Date: 13 September 2018

Accepted Date: 16 September 2018

Please cite this article as: Li W, Li Y, Liu Z, Kerdsakundee N, Zhang M, Zhang F, Liu X, Bauleth-Ramos Tomá, Lian W, Mäkilä E, Kemell M, Ding Y, Sarmento B, Wiwattanapatapee R, Salonen J, Zhang H, Hirvonen JT, Liu D, Deng X, Santos HéA, Hierarchical structured and programmed vehicles deliver drugs locally to inflamed sites of intestine, *Biomaterials* (2018), doi: https://doi.org/10.1016/j.biomaterials.2018.09.024.

Hierarchical structured and programmed vehicles deliver drugs locally to inflamed sites of intestine

Wei Li,[a1] Yunzhan Li,[b1] Zehua Liu,[a1] Nattha Kerdsakundee,[ac] Ming Zhang,[b] Feng Zhang,[a] Xueyan Liu,[b] Tomás Bauleth-Ramos,[ade] Wenhua Lian,[b] Ermei Mäkilä,[f] Marianna Kemell,[g] Yaping Ding,[a] Bruno Sarmento,[ad] Ruedeekorn Wiwattanapatapee,[c] Jarno Salonen,[f] Hongbo Zhang,[h] Jouni T. Hirvonen,[a] Dongfei Liu,*[ai] Xianming Deng,*[b] and Hélder A. Santos*[ai]

[a] Drug Research Program, Division of Pharmaceutical Chemistry and Technology, Faculty of Pharmacy, University of Helsinki, Helsinki 00014, Finland.

[b] State Key Laboratory of Cellular Stress Biology & Innovation Center for Cell Signaling Network and State-Province Joint Engineering Laboratory of Targeted Drugs from Natural Products and School of Life Sciences, Xiamen University, Xiamen 361102, Fujian, China.

[c] Department of Pharmaceutical Technology, Faculty of Pharmaceutical Sciences, Prince of Songkla University, 90110 Hat Yai, Thailand

[d] Instituto de Investigação e Inovação em Saúde (I3S), Instituto de Engenharia Biomédica (INEB), University of Porto, Rua Alfredo Allen, 208, 4200-135 Porto, Portugal

[e] Instituto Ciências Biomédicas Abel Salazar (ICBAS), University of Porto, Rua Jorge Viterbo 228, 4150-180 Porto, Portugal

[f] Laboratory of Industrial Physics, Department of Physics, University of Turku, Turku 20014, Finland

[g] Department of Chemistry, Faculty of Science, University of Helsinki, FI-00014 Helsinki, Finland

[h] Department of Pharmaceutical Sciences Laboratory & Turku Center for Biotechnology, Åbo Akademi University, Turku 20520, Finland

[i] Helsinki Institute of Life Science (HiLIFE), University of Helsinki, Helsinki 00014, Finland

Corresponding authors: dongfei.liu@helsinki.fi (D. Liu), xmdeng@xmu.edu.cn (X. Deng), helder.santos@helsinki.fi (H. A. Santos)

[1] These authors contributed equally to this work.

ABSTRACT

Orally administrable drug delivery vehicles are developed to manage incurable inflammatory bowel disease (IBD), however, their therapeutic outcomes are compromised by the side effects of systemic drug exposure. Herein, we use hyaluronic acid functionalized porous silicon nanoparticle to bridge enzyme-responsive hydrogel and pH-responsive polymer, generating a hierarchical structured (nano-in-nano-in-micro) vehicle with programmed properties to fully and sequentially overcome the multiple obstacles for efficiently delivering drugs locally to inflamed sites of intestine. After oral administration, the pH-responsive matrix protects the embedded hybrid nanoparticles containing drug loaded hydrogels against the spatially variable physiological environments of the gastrointestinal tract until they reach the inflamed sites of intestine, preventing premature drug release. The negatively charged hybrid nanoparticles selectively target the inflamed sites of intestine, and gradually release drug in response to the microenvironment of inflamed intestine. Overall, the developed hierarchical structured and programmed vehicles load, protect, transport and release drugs locally to inflamed sites of intestine, contributing to superior therapeutic outcomes. Such strategy could also inspire the development of numerous hierarchical structured vehicles by other porous nanoparticles and stimuli-responsive materials for the local delivery of various drugs to treat plenty of inflammatory gastrointestinal diseases, including IBD, gastrointestinal cancers and viral infections.

KEYWORDS

porous silicon; hybrid nanoparticle; stimuli responsive; targeting; drug delivery

1. Introduction

Inflammatory bowel disease (IBD), including ulcerative colitis and Crohn's disease, is chronic, relapsing and medically incurable inflammatory disorders of the intestine [1].

Current available therapies fail to adequately manage the IBD symptoms and are frequently associated with severe side effects resulting from systemic drug exposure [2]. One approach for more efficacious and safer IBD therapy could be nano/micro-vehicles mediated local drug delivery to achieve high drug concentration at the inflamed sites of intestine with minimal exposure of healthy intestine or distant tissues [3].

Drug delivery vehicles can rather easily reach inflamed intestine for local drug delivery by rectal administration which however leads to poor patient compliance [4-6]. For IBD therapy, patient compliance can never be overemphasized, which lies in the fact that incurable IBD, with most of the patients diagnosed under the age of 30, usually requires lifelong administration of drugs to manage symptoms [1]. Oral administration provides the greatest degree of patient compliance, however it makes the local drug delivery to inflamed intestine extremely challenging, as the corresponding drug delivery vehicles should fulfill multiple tasks during their journey from oral cavity to inflamed intestine. Specifically, an optimal vehicle should protect the drug and prevent premature drug release in the spatially variable physiological environments of the gastrointestinal (GI) tract, selectively target the discontinuously distributed inflamed sites of intestine which is usually surrounded by healthy intestine, and gradually release drug in response to the microenvironment of inflamed intestine.

To these ends, diverse vehicles, such as polymer particles [7-11], inorganic particles [12, 13], liposomes [14], solid lipid particles [15], and hydrogels [11, 16], have been developed. These vehicles, although are consisted of novel materials, have not demonstrated the ability to fully and sequentially overcome the multiple obstacles for delivering drugs locally to inflamed intestine, and their therapeutic outcomes, though encouraging, are still suboptimal and significantly compromised by the side effects of systemic drug exposure. Such frustrating situation prompts a rethink of the vehicle design strategy solely dependent on material composition, and raises attention to the structure design of vehicles for IBD therapy. A

hierarchical structured vehicle, with each level in its hierarchy being endowed by rational selected material with desired function, holds promise to sequentially tackle each of the multiple obstacles for local drug delivery to inflamed intestine.

Mesoporous nanoparticles, such as porous silicon (PSi), porous silica, halloysite, etc., are flexible in the loading/co-loading of drugs with different physicochemical properties [17-23], due to their tunable mesoporous structure, large pore volume and high specific surface area [24-26], and their hierarchized mesopores make them promising candidates for constructing hierarchical structured vehicles [22]. Mesoporous nanoparticles encapsulated in pH-responsive polymers (two levels of hierarchy) can deliver drugs to the desired segment of intestine, however the loaded drugs are usually rapidly released from mesopores nanoparticles in an uncontrolled manner due to their freely accessed pores [23, 27, 28]. Hydrogels formed by small molecules such as triglycerol monostearate (507 g mol^{-1}) and acorbyl palmitate (AP) (415 g mol^{-1}) can encapsulate drugs, and their enzyme-labile bonds enable gradual release of drugs in response to degradative enzymes, including matrix metalloproteinases (MMPs) and esterases [5, 29, 30], that are up-regulated and released in inflamed tissue [5, 29-34]. Inspired by these facts, we speculate that AP (molecule size ~2.60 nm [35]) can be co-loaded with drugs and further assembled with drugs into hydrogels inside the mesopores of PSi nanoparticles. The resultant AP loaded PSi nanoparticles are then expected to gradually release drugs in response to the microenvironment of inflamed intestine.

Furthermore, the versatile surface chemistry of PSi nanoparticles makes them a promising candidate for targeting the inflamed sites of intestine. Specifically, inflammation of the colon mucosa is accompanied by destruction and increased discontinuity of the mucus layer [36], and in situ accumulation of positively charged proteins including transferrin [14], eosinophil cationic protein [37] and bactericidal/permeability-increasing protein [38]. Consequently, positive charges build up on the surface of damaged epithelial offer a target for drug delivery

vehicles with negative surface charge [5, 14, 39]. Regarding PSi nanoparticles, negative charge can be readily obtained on their surface through surface modifications.

Here, we report a hierarchical structured vehicle (AP@PSi-HA@HPMCAS) based on hyaluronic acid (HA) functionalized PSi nanoparticles (PSi-HA), AP and hydroxypropyl methylcellulose acetate succinate (HPMCAS) with different solubility profiles depending on pH (LF, MF and HF grades) for efficient local drug delivery to inflamed intestine via oral administration. Budesonide (BUD), a glucocorticoid for IBD therapy [10], serves as a model drug in this study. AP and BUD are co-loaded and in situ gelled inside the mesopores of PSi-HA hybrid nanoparticles, and then delicately encapsulated in HPMCAS by microfluidic technique to form BUD loaded AP@PSi-HA@HPMCAS. We hypothesize that, after oral administration, pH-responsive HPMCAS matrix will prevent premature drug release from AP@PSi-HA nanoparticles in GI tract until they reach or are close to the inflamed sites of intestine. After the dissolution of HPMCAS, negatively charged AP@PSi-HA nanoparticles will then selectively bind to the inflamed sites of intestine by electrostatic adhesion, and then gradually release drug in response to inflammation due to the enzyme-labile bonds of AP (**Figure 1**). Overall, the hierarchical structured and programmable responsive AP@PSi-HA@HPMCAS will load, protect, transport and release drugs locally to inflamed sites of intestine after oral administration, and contribute to not only superior therapeutic efficacy but also considerably reduced systemic drug exposure.

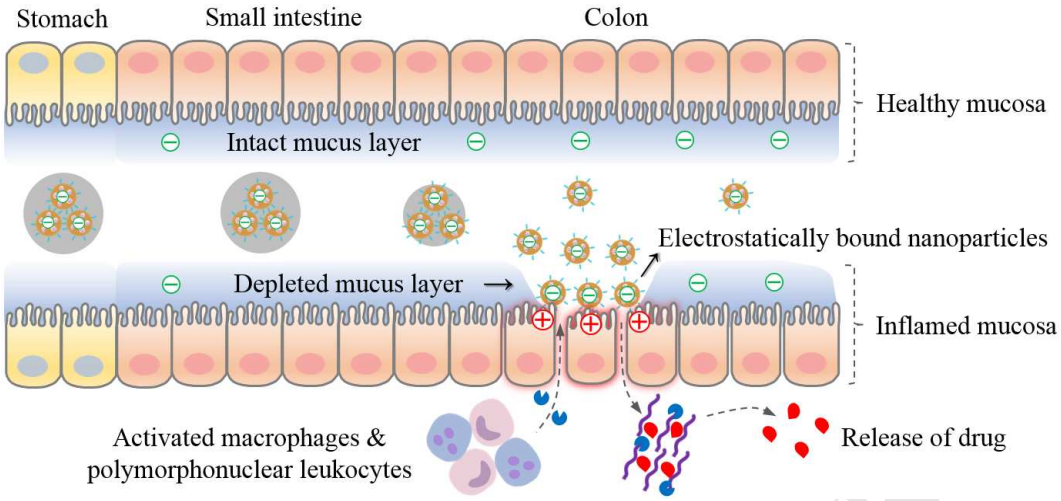

Figure 1. Proposed mechanism for the drug delivery by hierarchical structured and programed vehicles (AP@PSi-HA@HPMCAS) through GI tract with IBD. HPMCAS (LF, MF and HF grades), with different pH dissolution thresholds available, dissolves in specific segment of the GI tract. The released AP@PSi-HA nanoparticles with negative surface charge do not adhere to the intact mucosa, whereas only adhere to the inflamed mucosa which is characterized by depletion of mucus, accumulation of positively charged proteins, and enhancement of permeability of the epithelial cell layer. The degradative enzymes released by the inflamed cells degrade the AP hydrogel, which leads to the release of drug from AP@PSi-HA.

2. Results and discussion

The preparation process of the hierarchical structured and programmable responsive BUDAP@PSi-HA@LF for delivering BUD is schematically illustrated in **Figure 2**a. HA was conjugated onto the surface of carboxyl-terminated PSi nanoparticles (**Figure 2**b, **Figure S1**a) using spermine (SPM) as linker via 1-ethyl-3-(3-dimethylaminopropyl) carbodiimide/N-hydroxysuccinimide (EDC/NHS) reaction to form PSi-HA hybrid nanoparticles (**Figure 2**c, **Figure S1**b) with negative surface charge (–30 ± 2 mV) for targeting inflamed intestinal mucosa and high colloidal stability (**Figure 2**d–e) for microfluidic encapsulation. The successful conjugation of HA onto PSi was indicated by the particle size and surface charge

variations after each reaction step (**Figure 2**f), and confirmed by the appearance and enhancement of amide I band at 1642 cm^{-1} in the Fourier-transform infrared spectroscopy (FTIR) spectra (**Figure 2**g) after each reaction step in addition to the inheritance of characteristic bands of PSi, SPM and HA in PSi-HA (**Figure 2**g). The amount of HA in PSi-HA was determined to be 12.5 ± 1.3 wt% by thermogravimetric analysis (**Figure S2**). Small molecular BUD and AP were co-loaded into PSi-HA at 65 °C, and then were cooled down to room temperature for the in situ gelation of AP and BUD inside PSi-HA to form BUDAP@PSi-HA, making use of the readily temperature controlled gelation behavior of AP (**Figure S3)**. BUDAP@PSi-HA was subsequently encapsulated in LF to form the final hierarchical structured BUDAP@PSi-HA@LF particles (35 ± 1 µm) (**Figure 2**h) using droplet microfluidics. The obtained uniform particle size is beneficial for achieving controlled and reproducible drug release profiles [40]. The successful co-loading of BUD and AP in PSi-HA and encapsulation of BUDAP@PSi-HA in LF were confirmed by FTIR (**Figure S4**). The loading degree of BUD in BUDAP@PSi-HA and BUDAP@PSi-HA@LF was 24.5 ± 0.1 % and 3.8 ± 0.3 %, respectively.

The distribution of BUDAP@PSi-HA nanoparticles in the LF matrix was evaluated by confocal microscopy. To enable the visualization, PSi-HA was conjugated with fluorescein isothiocyanate (FITC, green) and LF matrix was labeled with tetramethylrhodamine (TRITC, red). The confocal images indicated that PSi-HA was evenly distributed in the LF matrix (**Figure 2**h), and scanning electron microscopy (SEM) image showed that BUDAP@PSi-HA@LF had smooth surface and well defined spherical shape (**Figure 2**h).

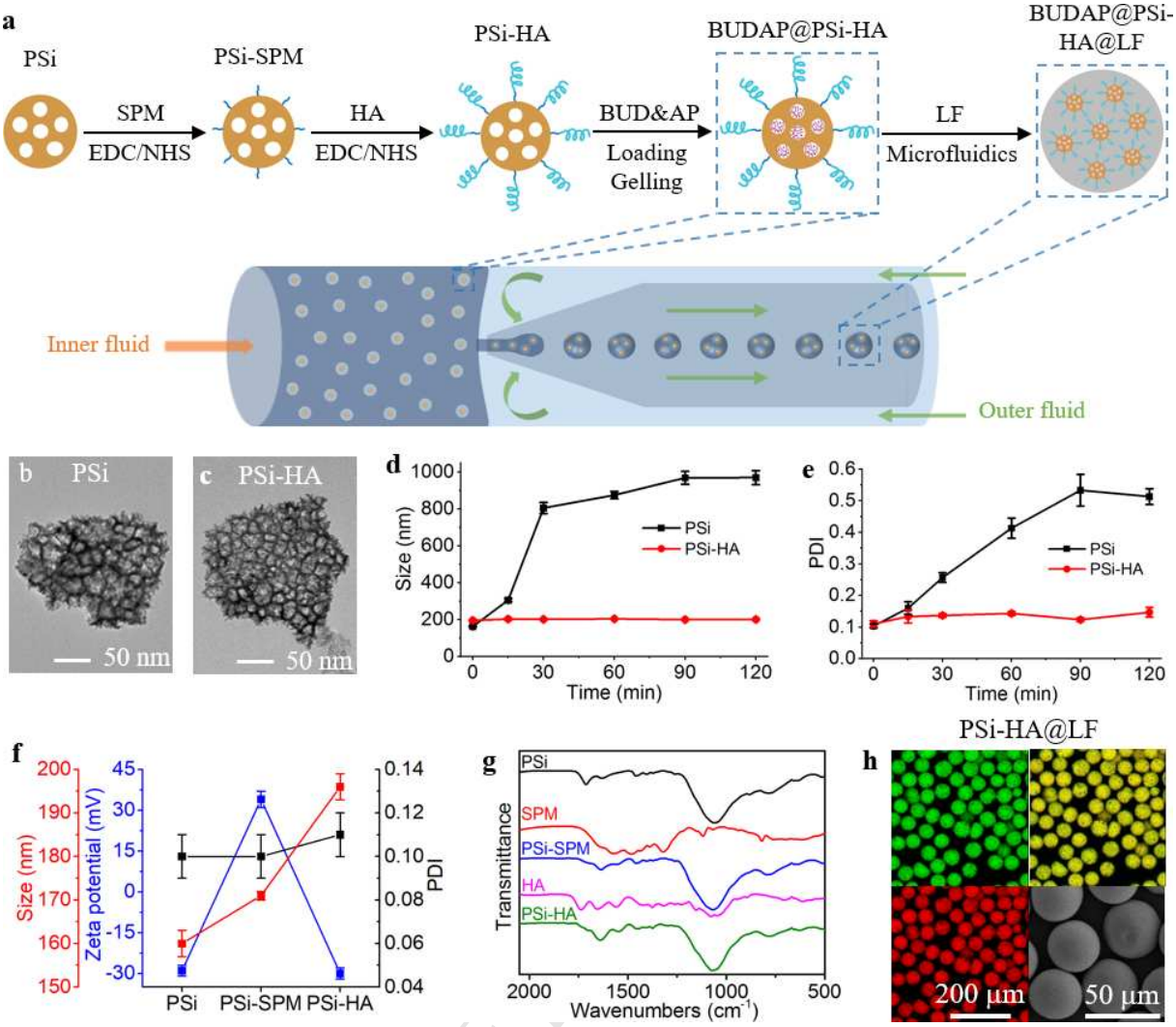

Figure 2. a) Fabrication process of hierarchical structured and programmable responsive vehicles (BUDAP@PSi-HA@LF). b–c) Transmission electron microscopy (TEM) image of b) PSi and c) PSi-HA. d) Size and e) polydispersity index (PDI) of PSi and PSi-HA dispersing in Milli-Q water during 2 h, demonstrating the high colloidal stability of PSi-HA over time. Data represent mean ± SD. (n = 3). f) Size, PDI, and surface zeta potential of PSi, PSi-SPM and PSi-HA. g) FTIR of PSi, SPM, PSi-SPM, HA and PSi-HA. h) The monodispersity of the fabricated BUDAP@PSi-HA@LF was studied by confocal microscopy and SEM. PSi-HA was conjugated with FITC and LF layer was labelled with TRITC. The confocal images showed the FITC (green), TRITC (red) and the overlay (yellow) channels. The surface of the particles was observed by SEM.

The developed hierarchical structured AP@PSi-HA@LF was then investigated for its programmable responsive properties. The pH-responsive dissolution behavior of protective matrix was firstly evaluated by immersing PSi-HA@LF in aqueous buffer solutions at various pH values, starting from pH 1.2 to 5.5. PSi-HA@LF was intact at pH < 5.5, and immediately began to dissolve at pH 5.5 (**Figure 3**a), while particles made by MF and HF only started to dissolve when pH reached 6.0 and 6.8, respectively [23, 41]. To further evaluate the pH-responsive properties of PSi-HA@HPMCAS (LF, MF or HF), BUD solely was loaded in PSi-HA@HPMCAS (LF, MF or HF). BUD@PSi-HA@LF, BUD@PSi-HA@MF and BUD@PSi-HA@HF only began to release BUD when the pH reached 5.5, 6.0 and 6.8, respectively, and the release was nearly complete within 30 min (**Figure S5**) due to the short disintegration time (~10 min according to the manufacturer) of HPMCAS (LF, MF and HF). The precisely pH-trigged drug release behaviors of PSi-HA@HPMCAS suggest its potential to release BUD at specific segment of the intestine by the flexible selection and combination of LF, MF and HF. The intestinal pH of mice is lower than that of human [42], therefore, LF rather than MF or HF was used for the animal experiments.

The enzyme-responsive properties of drug loaded AP@PSi-HA@LF were firstly investigated in buffer solutions. In contrast to the rapid release of BUD from PSi-HA@LF, AP@PSi-HA@LF only slightly released BUD (6.5% at 6 h) in the absence of lipase even though pH reached 5.5. With increasing concentration of lipase, gradual release of BUD from AP@PSi-HA@LF was accelerated, i.e., 8.5%, 75.6% and 88.4% at 6 h for 0.01, 1 and 100 U/mL lipase, respectively (**Figure 3**b), suggesting AP@PSi-HA@LF can adjust drug release to match the disease activity at inflamed intestine. IBD is characterized by variable disease activity over time with flares and periods of low disease activity. A disease activity-dependent drug delivery vehicle is likely to avoid sub- or supra-therapeutic drug concentrations locally during periods of high or low disease activity, respectively, resulting in maximized therapeutic efficacy and minimized systemic drug exposure [30].

Overall, BUDAP@PSi-HA@LF exhibited pH and enzyme programmable responsive drug release behaviors. To simulate drug release from AP@PSi-HA@LF under inflammatory conditions, BUDAP@PSi-HA@LF was incubated with supernatant collected from human macrophages cultured with or without lipopolysaccharide (LPS). In comparison to unstimulated macrophages, macrophages activated by LPS enhanced the enzymatic activities in the supernatant [5, 30, 32, 33], which resulted in significantly increased BUD release (**Figure 3**c). The above enzyme-responsive drug release behaviors suggest that AP@PSi-HA@LF would preferentially release BUD at the sites of inflamed intestine rather than healthy intestine or distant healthy tissues, and therefore reduce systemic drug exposure which often causes side effects.

Since AP@PSi-HA@LF is designed for oral drug delivery, two human intestinal epithelial cell lines, Caco-2 clone C2Bbe1 and HT29-MTX, were used to assess its safety. After 24 h incubation with both cell lines, there was no evidence of cytotoxicity for PSi-HA@LF and BUDAP@PSi-HA@LF as well as their components, i.e., PSi-HA, AP and BUD (**Figure S6, Figure S7** and **Figure S8**).

The therapeutic efficacy and systemic absorption of BUD delivered by AP@PSi-HA@LF were firstly studied using *in vitro* IBD model. The *in vitro* IBD model consisted of triple co-cultured cells including intestinal epithelial cells, human blood-derived macrophages and dendritic cells that were stimulated by pro-inflammatory cytokine interleukin-1β (IL-1β) in combination with lipopolysaccharide (LPS) (**Figure S9**). The experimental timeline of setting up the *in vitro* IBD model and subsequent testing of BUD formulations is shown in **Figure S10**. As an indication of the integrity and permeability of the monolayer, transepithelial electrical resistance (TEER) value was monitored during the experiment period. Compared to free BUD and BUD@PSi-HA@LF, BUDAP@PSi-HA@LF treatment recovered the TEER to the highest level, and was significantly higher at day 1 (**Figure S11**). Furthermore, as a marker of inflammation, IL-8 release from the cells under the treatment of different BUD

formulations was measured. BUDAP@PSi-HA@LF treatment significantly reduced the IL-8 production to the lowest level (**Figure 3**d), which indicates a prolong therapeutic effect of programmable responsive BUDAP@PSi-HA@LF than free BUD and BUD@PSi-HA@LF, mainly owing to the sustained drug release provided by the remaining enzyme-responsive BUDAP@PSi-HA on monolayers.

Since AP@PSi-HA@LF is designed for local delivery of BUD for precise therapy of IBD via oral administration, its effects on systemic drug absorption is another important evaluation index. AP@PSi-HA@LF significantly reduced the permeability of BUD across the monolayers in comparison to free BUD and PSi-HA@LF in both inflamed and healthy conditions (**Figure 3**e–f), which is attributed to the much slower release of BUD from AP@PSi-HA@LF (**Figure 3**b–c). Thus, delivering drug by hierarchical structured and programmable responsive AP@PSi-HA@LF will result in a major reduction in systemic drug absorption and consequently reduce the possibility of side effects.

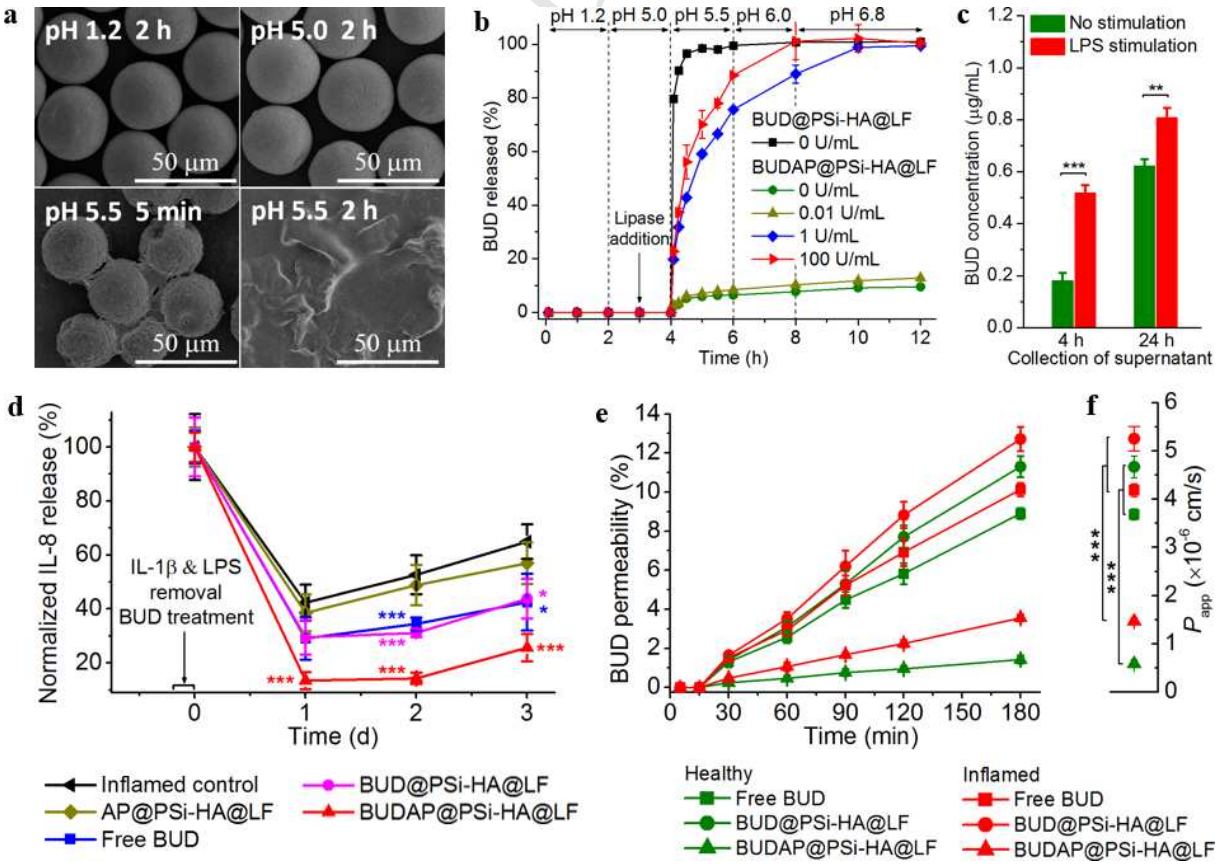

Figure 3. a) SEM images of PSi-HA@LF after immersion in buffer solutions at pH 1.2 and 5.0 for 2 h, and at pH 5.5 for 5 min and 2 h. b) pH and enzyme sequentially responsive BUD release from AP@PSi-HA@LF in a series of pH buffers at 37 °C. Enzyme (lipase; 0.01, 1, and 100 U/mL) was added at 3 h. Data are means ± SD (n = 3). c) BUD release from AP@PSi-HA@LF upon incubation for 24 h at 37 °C with culture supernatant from LPS activated human macrophages. Data are means ± SD (n = 3). d) Normalized IL-8 release of Caco-2 clone, macrophages and dendritic cells triple co-culture IBD model after induction of inflammation and subsequent treatment with various BUD formulations and blank vehicle control (without BUD). Data are means ± SD (n = 4). e) Permeation profiles of BUD across the Caco-2 clone monolayers co-cultured with macrophages and dendritic cells in both healthy and inflamed conditions. f) Apparent permeability coefficients (P_{app}) of BUD calculated from the permeation profiles of BUD. Data are means ± SD (n = 3).

To maximize the therapeutic efficacy and minimize the systemic exposure of drug delivered by AP@PSi-HA@LF *in vivo*, AP@PSi-HA@LF should selectively adhere to the inflamed sites of intestine. We hypothesize that the negative surface charge of AP@PSi-HA (–32 ± 1 mV) will facilitate its targeting to the inflamed intestinal epithelium, where positively charged proteins are accumulated [14, 37, 38]. To verify this hypothesis, the adhesion properties of AP@PSi-HA were firstly tested *in vitro* using synthetic surfaces. BUDAP@PSi-FITC/HA (–33 ± 2 mV) was incubated on glass slides or polystyrene plates coated with human transferrin (positively charged) or porcine mucin (negatively charged), simulating inflamed and healthy epithelium, respectively [5]. Compared to mucin coated surfaces, transferrin coated surfaces retained much more particles (**Figure 4**a) and showed a 14.9-fold higher fluorescence signal (**Figure 4**b) after extensive washing with phosphate buffered saline (PBS). In another control experiment, BUDAP@PSi-FITC/HA was incubated with a cationic polyethylenimine (PEI) solution to convert its surface charge from negative to positive (35 ± 2 mV). As predicted, this

charge conversion abolished the preferential adhesion of BUDAP@PSi-HA to transferrin coated surfaces and enhanced its adhesion to the mucin coated surfaces (**Figure S12**).

Following the promising results *in vitro*, we further examined the targeting of AP@PSi-HA to inflamed mucosa using *in vivo* IBD model, i.e., dextran sulfate sodium (DSS)-induced mouse colitis model. Mice with colitis and normal mice received a single dose of BUDAP@PSi-Cy7/HA@LF (–31 ± 1 mV for BUDAP@PSi-Cy7/HA) (for IVIS imaging) or BUDAP@PSi-FITC/HA@LF (for confocal imaging) by oral gavage. Mice with colitis showed significantly greater retention of fluorescence than normal mice after the administration of BUDAP@PSi-Cy7/HA@LF for 2 h and 5 h (**Figure 4**c and **Figure 4**d). Confocal microscopy images of distal end of colon sections (**Figure 4**e) showed the targeting of BUDAP@PSi-FITC/HA to the inflamed sites of colon. Together with the pH and enzyme responsive properties of AP@PSi-HA@LF, we would expect that hierarchical structured AP@PSi-HA@LF can efficiently deliver BUD locally to inflamed sites of intestine by executing its programmed functions in the GI tract suffered with IBD.

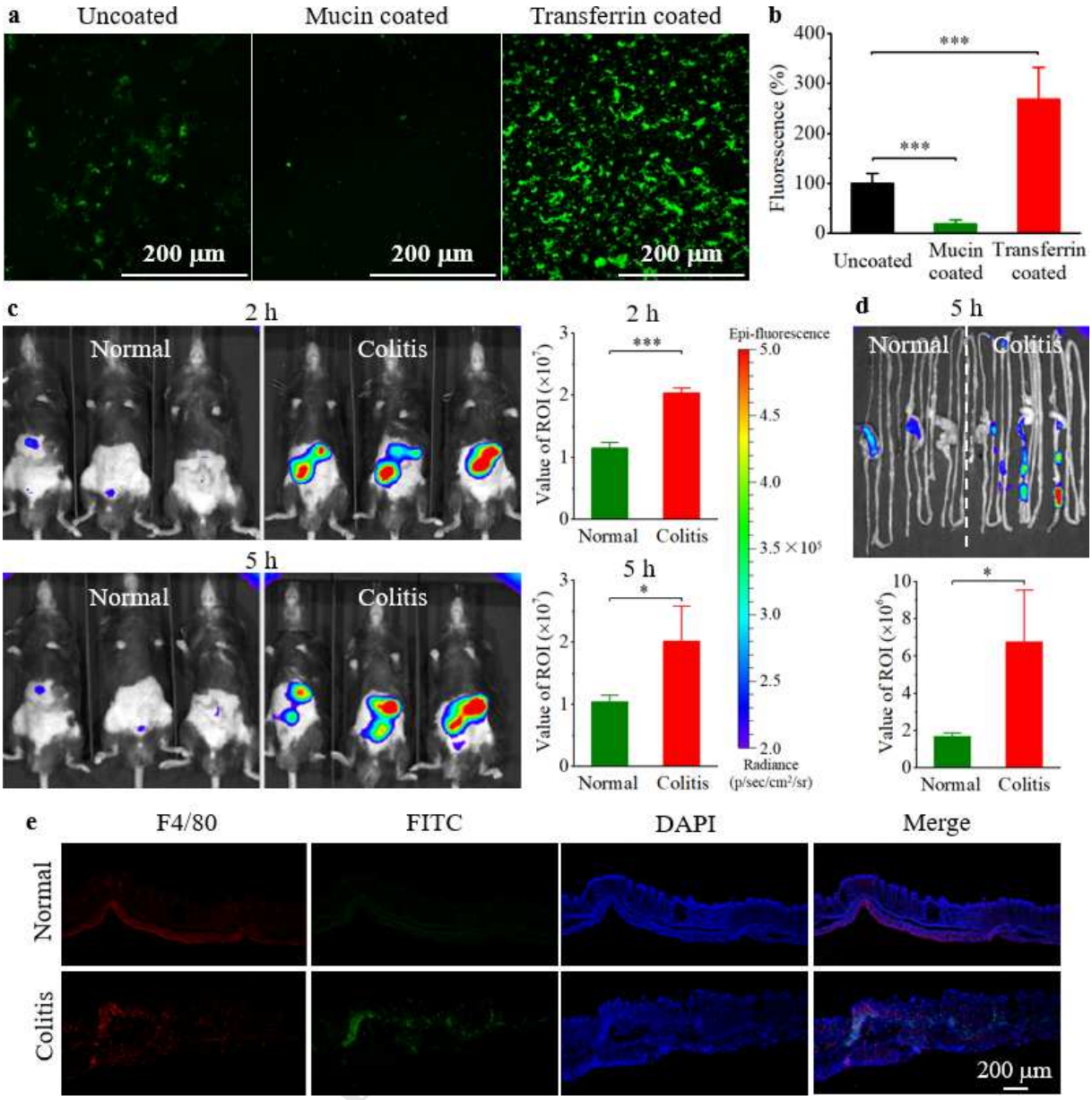

Figure 4. a) Confocal microscopy images and b) fluorescence intensities (quantified by microplate reader) of BUDAP@PSi-FITC/HA after incubation with uncoated, mucin coated (simulating healthy epithelium) or transferrin coated (simulating inflamed epithelium) surfaces for 1 h at 37 °C, followed by washing with PBS for 3 times. Data are means ± SD (n = 6). c–d) Mice with DSS-induced colitis and normal mice were orally administrated with BUDAP@PSi-Cy7/HA@LF. c) The living mice were imaged using IVIS fluorescence imaging system after 2 h and 5 h, respectively. d) The mice were sacrificed 5 h after administration, and the intestines were dissected and imaged using IVIS fluorescence imaging system. The total fluorescence intensity was determined in a standard-size region of interest

(ROI) drawn around the whole intestine (c) or colon (d). (c) and (d) share the same radiance scale bars. Data are means ± SD (n = 3). e) Immunofluorescence images of distal end of colon dissected from normal mice and mice with colitis 5 h after orally administrated with BUDAP@PSi-FITC/HA@LF. Nucleus and macrophages were stained by DAPI and F4/80, respectively. All the images have the same scale bar.

We then tested the *in vivo* therapeutic efficacy of BUD delivered by hierarchical structured and programmable responsive AP@PSi-HA@LF in DSS-induced mouse colitis model. BUD was studied at low dose (L, 0.5 mg/kg) and high dose (H, 1.5 mg/kg), respectively. Free BUD (FBUDL and FBUDH), blank vehicles without BUD, *i.e.*, AP@PSi-HA@LF (PL and PH) and pH-responsive BUD@PSi-HA@LF (BUDL and BUDH) were employed as controls to demonstrate the therapeutic benefits of hierarchical structured and programmable responsive BUDAP@PSi-HA@LF (BUDAPL and BUDAPH). After induction of the colitis for 7 d, the treatment was conducted by daily oral gavage for 7 d, during which the body weight of colitis mice gradually decreased (**Figure 5**a). Whereas treatment with BUDAP@PSi-HA@LF (BUDAPL and BUDAPH) significantly mitigated weight loss as compared to free BUD (FBUDL and FBUDH) and BUD@PSi-HA@LF (BUDL and BUDH) (**Figure 5**a). The severity of colitis was assessed by disease activity index (DAI). Interestingly, all treated groups showed significantly reduced DAI after treatment for 7 d as compared to colitis group, and the minimal DAI was found for BUDAP@PSi-HA@LF (BUDAPL and BUDAPH) (**Figure 5**b). Besides, BUDAPH notably preserved colon length when compared to FBUDH and BUDH (**Figure S13**). Furthermore, the levels of typical proinflammatory cytokines including IL-1β and IL-6 were quantified. Colitis mice exhibited elevated levels of both IL-1β and IL-6 than normal mice (**Figure 5**c–d). Overall, the levels of IL-1β and IL-6 decreased after treatment with BUD formulations, and the group of mice treated with BUDAP@PSi-

HA@LF showed the lowest concentration of IL-1β and IL-6 in comparison to the other treated groups.

Additional information was obtained by examining and scoring hematoxylin and eosin (H&E) stained histological sections of distal end (**Figure 5**e–f) of colon tissues. The colitis was characterized by superficial erosions, depletion of goblet cells, infiltration of the colon lamina propria with inflammatory cells, and crypt hypertrophy [5, 9]. Disease severity was significantly reduced in mice treated with BUD@PSi-HA@LF (BUDL and BUDH) and BUDAP@PSi-HA@LF (BUDAPL and BUDAPH) (**Figure 5**e), and representative images (**Figure 5**f) demonstrate that treatment with BUDAP@PSi-HA@LF offered the best improvement in pathological injuries, which was also confirmed by TUNEL staining (**Figure S14**). Overall, BUD delivered by hierarchical structured and programmable responsive AP@PSi-HA@LF exhibits superior therapeutic efficacy than free BUD and BUD delivered by pH-responsive PSi-HA@LF, which was attributed to the protection of BUDAP@PSi-HA in GI tract by LF, targeting of BUDAP@PSi-HA to the inflamed sites of colon and subsequent prolonged release of BUD from AP@PSi-HA in response to the microenvironment of inflamed intestine.

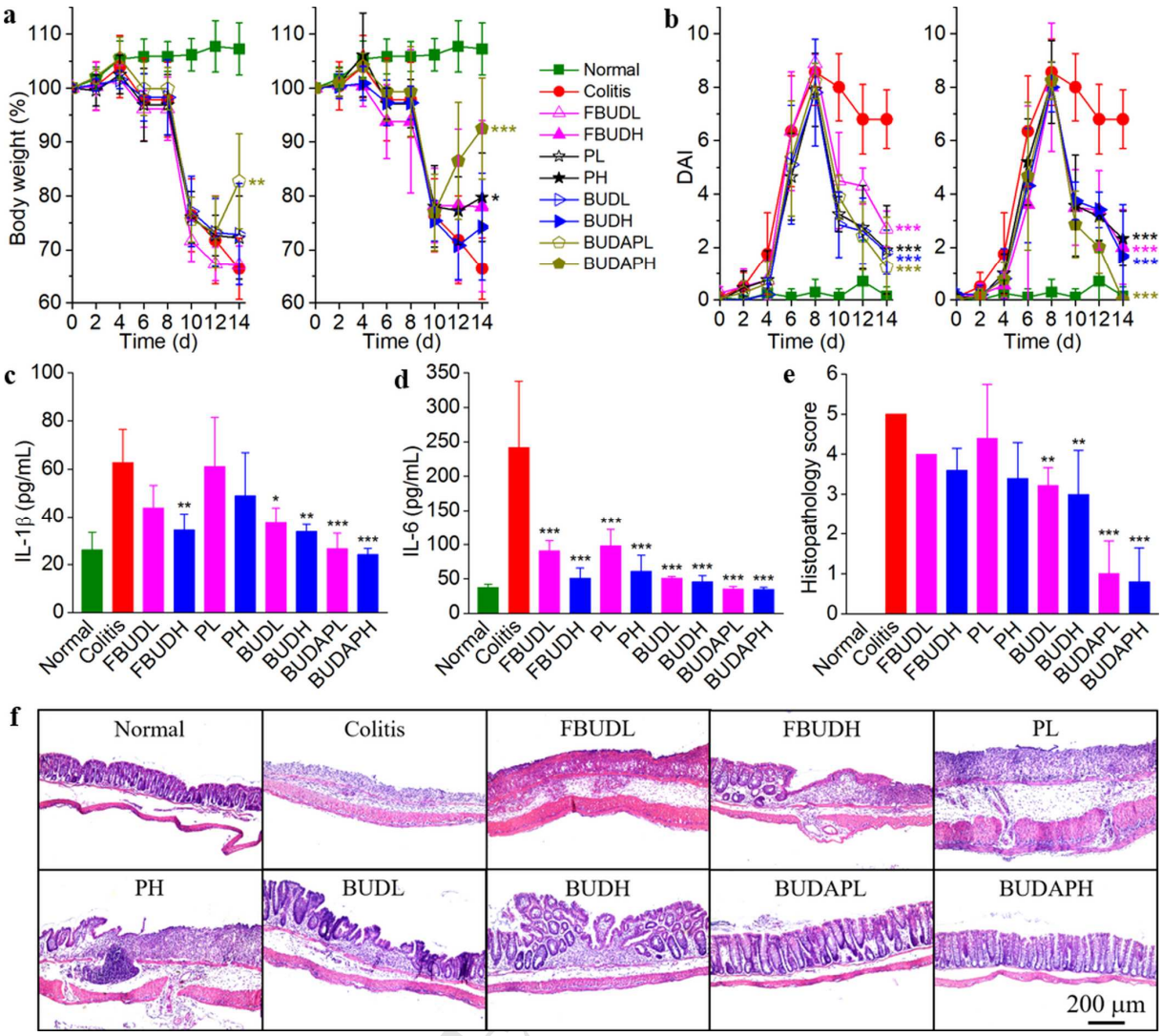

Figure 5. Therapeutic efficacy of various BUD formulations on IBD model of DSS-induced colitis in mice. a) Body weight and b) DAI of mice during 7 d of induction of colitis model and 7 d of treatment. Data were normalized as a percentage of the body weight at day 0. c–d) The levels of c) IL-1β and d) IL-6 after 7 d of treatment. e) Histopathology score of the distal end of colon after 7 d of treatment. f) Representative H&E histology images of the distal end of colon after 7 d of treatment. All the images have the same scale bar. Data are means ± SD (n = 5). *p < 0.05, **p < 0.01 and ***p < 0.001 versus the colitis group.

3. Conclusions

In summary, we have developed a hierarchical structured and programmable responsive AP@PSi-HA@HPMCAS vehicle for efficient local drug delivery to inflamed sites of

intestine in IBD therapy via oral administration. The prepared vehicles showed well-defined spherical shape and uniform particle size. The pH-responsive matrix protects the drug and AP co-loaded PSi nanoparticles against the complex environment of the GI tract before reaching the desired segment of intestine, and prevents premature drug release. The negatively charged AP@PSi-HA nanoparticles selectively target the inflamed sites of intestine, and locally release the drug in response to the inflammation gradually over a prolonged duration. Compared to free drug and conventional pH-responsive particles, drug delivered by hierarchical structured and programmable responsive AP@PSi-HA@HPMCAS exhibit superior therapeutic efficacy and significantly reduced systemic drug exposure, substantiating the importance of engineering hierarchical structured and programmed vehicles for delivering drugs locally to inflamed sites of intestine.

4. Materials and methods

4.1. Preparation of PSi nanoparticles

Electrochemical anodization method was used to prepare undecylenic acid modified thermally hydrocarbonized PSi (UnTHCPSi), as described in detail elsewhere [43]. Briefly, monocrystalline p+-type Si (100) wafers (0.01–0.02 Ω cm resistivity) were electrochemically anodized in a 1:1 (v/v) aqueous hydrofluoric acid (38%)–ethanol electrolyte by applying repeated low and high current density pulsed etching profile. The resulting PSi with high porosity fracture planes and hydrogen-terminated surface was subsequently detached from the substrate as free-standing multilayer films by abruptly increasing the current density to electropolishing region. Thermal hydrocarbonization of the PSi films was performed by exposing them to a 1:1 (v/v) N_2/acetylene (C_2H_2) flow (1 L min^{-1}) for 15 min at room temperature, followed by a heat treatment for 15 min at 500 °C. The obtained THCPSi films were then treated with 10-undecenoic acid for 16 h at 120 °C. The UnTHCPSi films were finally wet ball milled to produce nanoparticles and separated using centrifugation to obtain

the final PSi nanoparticles with desired particle size. Nitrogen adsorption–desorption isotherms of PSi nanoparticles were measured at 77 K on a gas adsorption analyzer (Micromeritics TriStar 3000, USA). The specific surface area was determined from the adsorption branch of the nitrogen isotherm using the Brunauer-Emmett-Teller (BET) theory [44], and the pore volume was determined as the total adsorbed amount at a relative pressure (p/p_0) of 0.97. The average diameter of the pores was 4×pore volume/specific surface area. The specific surface area and pore volume of PSi nanoparticles used in this study were 305 ± 10 m^2/g and 0.89 ± 0.01 cm^3/g, respectively. The average diameter of the pores was calculated to be 11.6 ± 0.4 nm.

4.2. Preparation of HA

The aqueous solution of HA sodium salt (Sigma-Aldrich, USA) was dialyzed against 0.01 M HCl for 24 h and then against Milli-Q water for an additional 24 h to convert HA from its sodium salt form to acid form. The acid form of HA was recovered by lyophilization [45].

4.3. Preparation of PSi-HA nanoparticles

PSi nanoparticles were covalently conjugated with SPM using the EDC/NHS reaction. Typically, 1 mg PSi nanoparticles were dispersed in 1 mL of anhydrous dimethylformamide (DMF) (Sigma-Aldrich, USA). Then 4 μL (22.6 μmol) EDC (Sigma-Aldrich, USA) and 3 mg (26.1 μmol) NHS (Sigma-Aldrich, USA) were added into the above suspension and stirred overnight. Subsequently, 20 mg (98.8 μmol) SPM (ACROS Organic, UK) were added and stirred overnight. The prepared PSi-SPM nanoparticles were collected by centrifugation and extensively washed with DMF for 3 times. 4 mg HA were dissolved in 1 mL anhydrous dimethyl sulfoxide (DMSO) (Sigma-Aldrich, USA). Then 2.8 μL EDC and 1.8 mg NHS were added and stirred for 2 h. Afterwards, 1 mg PSi-SPM nanoparticles were dispersed into the above solution and stirred overnight. The obtained PSi-HA nanoparticles were collected by centrifugation and extensively washed with Milli-Q water for 5 times.

The amount of HA on the surface of PSi nanoparticles was estimated using TGA 7 thermogravimeter (PerkinElmer, USA). The samples were heated from room temperature to 850 °C at a heating rate of 20 °C /min under a 200 mL/min N_2 flush. The measurements were done in triplicates.

4.4. Loading of BUD and AP in PSi-HA nanoparticles

BUD and AP were co-loaded into PSi-HA nanoparticles using an immersion method. BUD and AP were dissolved together in a mixture of ethanol–H_2O (1:1 v/v) at a concentration of 25 and 75 mg/mL, respectively, at 65 °C. 10 mg PSi-HA were added into 2 mL of the above solution and stirred for 3 h at 65 °C. Afterwards, the BUD and AP loaded PSi-HA (BUDAP@PSi-HA) nanoparticles were collected by centrifugation for 3 min using pre-warmed rotor, and then were allowed to cool down to room temperature for the gelling of AP before washing by Milli-Q water. The procedures to prepare PSi-HA loaded with BUD only (BUD@PSi-HA) and PSi-HA loaded with AP only (AP@PSi-HA) were the same as BUDAP@PSi-HA, and the concentration of BUD and AP in ethanol–H_2O (1:1 v/v) was 25 and 75 mg/mL, respectively.

4.5. Fabrication of flow-focusing device for microfluidics

Borosilicate glass cylindrical capillaries (World Precision Instruments, USA) and glass slides were used to assemble the microfluidic flow-focusing device [23, 27]. The inner capillary had an outer diameter of 1000 µm. Firstly, the inner capillary was tapered using a micropipette puller (P-97, Sutter Instrument, USA), and then enlarged to 350 µm. Subsequently, the tapered capillary was inserted into the right end of the outer capillary with an inner diameter of 1120 µm. Two syringes were linked to the microfluidic device using polyethylene tubes to allow the independent injection of the inner and outer fluids controlled by pumps (PHD 2000, Harvard Apparatus, USA). A transparent epoxy resin (5 minute® Epoxi, Devcon, USA) was used to seal the microfluidic device where required.

4.6. Fabrication of pH-responsive microparticles

PSi-HA nanoparticles were encapsulated in pH-sensitive HPMCAS (ShinEtsu, Japan) to form PSi-HA@HPMCAS microparticles using water-in-oil-in-water (W/O/W) double emulsion through a microfluidic flow-focusing device. Three grades (LF, MF and HF) of HPMCAS, which vary in their pH-dependent solubility, were used. The LF, MF and HF grades of HPMCAS dissolve at pH ≥ 5.5, 6.0 and 6.8, respectively. For the microfluidic encapsulation, HPMCAS (LF, MF or HF) was dissolved in ethyl acetate (EA) at a concentration of 10 mg mL^{-1}. 2 mg PSi-HA nanoparticles were dispersed in 100 μL Milli-Q water and added dropwise into 1 mL HPMCAS (LF, MF or HF) solution under sonication (Sonics, Sonics & Materials Inc, USA) to produce the primary emulsion (W/O) which served as the inner dispersed fluid. 2% w/v P-407 (BASF, Germany) aqueous solution (pH 5) was used as the outer continuous fluid to obtain a stable W/O/W emulsion. The inner fluid (3.5 mL h^{-1}) was focused by the outer fluid (15 mL h^{-1}), and the formed droplets were collected in 1% w/v P-407 aqueous solution (pH 5). Afterwards, the produced PSi-HA@HPMCAS (LF, MF or HF) microparticles were collected by centrifugation.

4.7. Fabrication of BUD and/or AP loaded microparticles

BUDAP@PSi-HA@LF, BUD@PSi-HA@HPMCAS (LF, MF or HF) and AP@PSi-HA@LF microparticles were prepared using BUDAP@PSi-HA, BUD@PSi-HA and AP@PSi-HA nanoparticles, respectively, under the same condition as the PSi-HA@LF microparticles. The loading degrees of BUD in particles were determined by stirring the particles in a mixture of PBS and acetonitrile (1:1 v/v) to dissolve the HPMCAS matrix and AP hydrogel, and to release all the loaded BUD. The amount of BUD was quantified by Agilent 1100 high performance liquid chromatography (HPLC) (Agilent Technologies, USA) with a mobile phase composed of phosphoric acid (0.1%, pH 3.2) and acetonitrile (volume ratio 52:48) at a flow rate of 1.4 mL min^{-1} at 25 °C. The wavelength used for BUD quantification was 244 nm.

A Discovery® C18 column (4.6 × 150 mm, 5 µm, Supelco Analytical, USA) was used as stationary phase and the injection volume of the samples was 20 µL.

4.8. Physicochemical properties of nanoparticles and microparticles

The particle size, PDI and surface charge of nanoparticles were determined by Zetasizer Nano ZS (Malvern Instruments Ltd, UK) in Milli-Q water with pH adjusted to 7.4 by HCl/NaOH.

The stability of nanoparticles was evaluated by following their changes on size and PDI after incubation of 200 µg/mL of nanoparticles with Milli-Q water (pH 7.4) during 2 h. Samples were withdrawn at 15, 30, 60, 90 and 120 min, and diluted in Milli-Q water (pH 7.4) for measuring the size and PDI. Milli-Q water was used for stability test as it was used for dispersing the PSi-HA nanoparticles during the microfluidic fabrication of PSi-HA@HPMCAS.

The structure of nanoparticles and morphology of microparticles were observed by TEM (JEOL 1400, Japan) and SEM (Hitachi S-4800, Japan), respectively. The microparticles were platinum sputtered before imaging. The particle size of microparticles was determined using Image J (NIH, USA), and at least 100 particles were analyzed. The chemical composition of the nanoparticles and microparticles was characterized by FTIR (Vertex 70, Bruker, USA). The samples were mixed with KBr (FTIR grade, Sigma-Aldrich, USA) and pressed into pellets. The pellets consisted of 1 mg of sample and 200 mg of KBr. The FTIR spectra were recorded in the range of 4000–400 cm^{-1} with a resolution of 4 cm^{-1} using OPUS 5.5 software.

For studying the distribution of PSi-HA nanoparticles within the LF microparticles, PSi-HA was labelled with FITC (Thermo Fisher Scientific, USA) as described in following sections, and the LF polymer was mixed with TRITC (Thermo Fisher Scientific, USA) at a mass ratio of 100 to 1. After microfluidic fabrication as described above, the produced PSi-HA@LF microparticles were placed into 35 mm Petri dish (MatTek, USA), and imaged using confocal microscope (Leica SP5 II HCS A, Germany).

4.9. pH-responsive dissolution behavior of microparticles

To investigate the pH-responsive dissolution behavior of the prepared PSi-HA@LF microparticles, they were mounted onto stubs using carbon tape, and then treated with buffer solutions at different pH values (1.2 and 5.0) for 2 h and at pH 5.5 for 5 min and 2 h. The excess solutions were removed and the samples were dried at room temperature for 24 h. The microparticles without any treatment were used as a control. All samples were platinum sputtered before imaging.

4.10. pH-responsive drug release study

The pH-responsive drug release profiles of BUD@PSi-HA@HPMCAS (LF, MF and HF) were studied in continuous gradient pH media at 37 °C with shaking at 150 rpm. Free BUD was used as control group. Samples containing 50 μg BUD were added into 50 mL media at pH 1.2, and the pH was then gradually increased to 5.0, 5.5, 6.0 and 6.8. At predetermined time intervals, 200 μL of sample were withdrawn from each sample and the release media was replaced with 200 μL of fresh media. Samples were firstly centrifuged (16100 g, 3 min), and then the drug concentrations in the supernatant were quantified by HPLC.

4.11. Enzyme-responsive drug release study

The enzyme-responsive drug release profiles of BUDAP@PSi-HA@LF were studied in continuous gradient pH media without and with 0.01, 1 or 100 U/mL of *Thermomyces lanuginosus* lipase (Sigma-Aldrich, USA) at 37 °C with shaking at 150 rpm. BUD@PSi-HA@LF and free BUD were used as control groups. Samples containing 50 μg BUD were added into 50 mL media at pH 1.2, and the pH was then gradually increased to 5.0, 5.5, 6.0 and 6.8. Lipase was added when pH was increased to 5.0. At predetermined time intervals, 200 μL of sample were withdrawn from each sample and the release media was replaced with

200 μL of fresh media. Samples were firstly centrifuged (16100 g, 3 min), and then the drug concentrations in the supernatant were quantified by HPLC.

BUD release was also studied in culture supernatant from human macrophages. The method for obtaining macrophages was described in detail in later sections. Macrophages were cultured without and with 0.1 μg/mL lipopolysaccharide (LPS) (Sigma-Aldrich, USA), and supernatant was collected after 4 and 24 h. 10 mg BUDAP@PSi-HA@LF were suspended in 1 mL of Milli-Q water (pH 5.0), and 20 μL of this suspension were added to 1 mL of supernatant from unstimulated or LPS-stimulated macrophages. After incubation at 37 °C for 24 h, samples were centrifuged at 16100 g for 5 min, and BUD concentration in the supernatant was measured by HPLC.

4.12. Cell line culture

Human colon carcinoma (Caco-2), Caco-2 clone C2Bbe1 and human colon adenocarcinoma (HT29-MTX) cells were separately cultured in Dulbecco's modified Eagle medium (DMEM) (HyClone, USA) with 4.5 g L^{-1} glucose, supplemented with 10% fetal bovine serum (Gibco, Invitrogen, USA), 1% nonessential amino acids, 1% L-glutamine, penicillin (100 IU mL^{-1}) and streptomycin (100 mg mL^{-1}) (all from HyClone, Logan, UT). The cells were maintained at 37 °C with an atmosphere of 5% CO_2 and 95% relative humidity, and the culture media were changed every other day. Prior to each test, the cells were harvested using 0.25% (v/v) trypsin–ethylenediaminetetraacetic acid (EDTA)–phosphate buffer solution.

4.13. Macrophages and dendritic cells culture

Buffy coats were processed by Ficoll-Paque gradient centrifugation to obtain the peripheral blood mononuclear cells (PBMCs). Macrophages and dendritic cells were differentiated from $CD14^+$ monocytes that were isolated from PBMCs using CD14 MicroBeads (Miltenyi Biotec). These cells were cultured with macrophage medium (RPMI 1640 medium with 1% L-glutamine (HyClone, USA), supplemented with 10% human serum AB (BioWest, France),

1% nonessential amino acids, penicillin (100 IU mL^{-1}) and streptomycin (100 mg mL^{-1}), and 1% sodium pyruvate (Gibco, UK)). Macrophages were obtained after cultivation for 6 d with macrophage medium, while dendritic cells were obtained after cultivation for 6 d with macrophage medium supplemented with 80 ng/mL recombinant human GM-CSF (Peprotec, USA) and 80 ng/mL recombinant human IL-4 (Peprotec, USA) [46].

4.14. Cytotoxicity studies

100 µL Caco-2 clone and HT29-MTX cells were separately seeded in 96-well plates at a density of 2×10^5 cells mL^{-1}. After the cells were left to attach for 24 h, the culture medium was discarded and the cells were washed with 100 µL fresh 1× Hank's Balanced Salt Solution (HBSS)–HEPES (pH 7.4). Then PSi, PSi-HA and PSi-HA@LF at concentrations of 25, 50, 100, 250 and 500 µg mL^{-1} (PSi or equivalent) in HBSS–HEPES (pH 7.4), AP at concentrations of 5, 10, 25, 50 and 100 µg mL^{-1} in HBSS–HEPES (pH 7.4), and free BUD, BUDAP@PSi-HA and BUDAP@PSi-HA@LF at concentrations of 5, 10, 20, 50 and 100 µg mL^{-1} (BUD or equivalent) in HBSS–HEPES (pH 7.4) were added to each well. After incubation for 24 h, the cells were washed twice with HBSS–HEPES (pH 7.4) and the number of viable cells was quantified using CellTiter-Glo® (Promega Corporation, USA). The luminescence was measured using Varioskan Flash plate reader (Thermo Fisher Scientific, USA). HBSS–HEPES (pH 7.4) and 1% of Triton X-100 were used as negative control and positive control, respectively. All the experiments were performed at least in triplicate.

4.15. In vitro IBD model

In vitro IBD model was modified from previous studies [47-49]. 6×10^4 Caco-2 clone cells were seeded into the apical compartment of 12-Transwell® plate, 1×10^4 macrophages and 1×10^4 dendritic cells were seeded into the basolateral compartment. The co-culture was kept with Caco-2 medium (0.5 mL) in the apical compartment and macrophage medium (1.5 mL)

in the basolateral compartment, and the medium was changed every other day in both the apical and basolateral compartments. The co-culture was cultivated for 21 d to form cell monolayers. For the inflamed model, 0.5 mL Caco-2 medium with 20 ng mL^{-1} IL-1β (Peprotec, USA) and 0.1 μg mL^{-1} LPS was added to the apical compartment and incubated for 2 d.

4.16. Drug permeability across intestinal cell monolayers

The permeability experiments were performed using *in vitro* IBD model at 37 °C with shaking at 100 rpm, in comparison with healthy intestinal cell monolayers. After 2 d of cultivation with or without stimulation, the medium from the apical compartment was collected for dispersing the samples. 500 μL free BUD, BUD@PSi-HA@LF and BUDAP@PSi-HA@LF in apical medium were added into the apical compartment at a BUD (or equivalent) concentration of 50 μg mL^{-1}. At specific time points (5, 15, 30, 60, 90, 120 and 180 min), 100 μL sample were collected from the basolateral compartment and replaced with the same volume of fresh medium. The amount of permeated BUD in the basolateral compartment was quantified by HPLC, and the P_{app} was calculated, as described elsewhere [20]. The experiments were carried out in triplicate.

4.17. In vitro treatment tests

After 2 d of stimulation, both apical and basolateral medium were removed, and cells were washed 3 times with PBS. Free BUD, BUD@PSi-HA@LF and BUDAP@PSi-HA@LF were added into the apical compartment, providing an equivalent BUD dose of 25 μg per well. After 4 h of incubation, which approximates drug retention time in the intestine of IBD patients [50], the apical medium was removed and replaced with fresh Caco-2 medium. The monolayers were used both for transepithelial electrical resistance (TEER) and IL-8 measurements. IL-8 was quantified by enzyme-linked immunosorbent assay (ELISA) kits (BD Biosciences) according to the manufacturer's protocol.

4.18. Fluorescence labelling of nanoparticles

FITC labelled PSi-SPM (PSi-FITC) and Cy7 labelled PSi-SPM (PSi-Cy7) were prepared by overnight stirring of 10 mg of PSi-SPM with 0.1 mg of FITC-NHS (Thermo Fisher Scientific, USA) and 0.1 mg of Cy7-NHS (Lumiprobe, Germany) in DMF, respectively. The obtained PSi-FITC and PSi-Cy7 were conjugated with HA using the EDC/NHS reaction as described above to produce FITC labelled PSi-HA (PSi-FITC/HA) and Cy7 labelled PSi-HA (PSi-Cy7/HA), respectively.

4.19. In vitro adhesion of nanoparticles

FITC labelled PSi-HA were used for imaging in all *in vitro* adhesion experiments. Healthy and inflamed mucosa were simulated by coating Lab-Tek™ 8-chamber slides (Thermo Fisher Scientific, USA) or 96-well polystyrene plates (Corning, USA) with mucin from porcine stomach (Sigma-Aldrich, USA) and human transferrin (Sigma-Aldrich, USA), respectively [5]. Briefly, mucin solution (30 mg/mL in HBSS) was added to the chamber slides/plates and incubated at room temperature for 2 h with gentle shaking. Transferrin solution (500 µg/ml in PBS) was added to the chamber slides/plates and incubated overnight at 37 °C. Chamber slides/plates incubated with PBS overnight at 37 °C were used as uncoated chamber slides/plates. After incubation, chamber slides/plates were washed with PBS for 3 times. FITC labelled BUDAP@PSi-HA were dispersed in PBS at a concentration of 50 µg/ml, and then added to each well of the chamber slides/plates. The chamber slides/plates were gently shaken at room temperature for 1 h. Wells were then washed with PBS for 3 times. The chamber slides were imaged using confocal microscope (Leica TCS SP5 II HCS A, Germany), and the fluorescence intensities of the plates were quantified using Varioskan™ LUX (Thermo Fisher Scientific, USA).

In a second set of experiments, cationic branched polyethylenimine (PEI) (~25,000 g/mol, Sigma-Aldrich, USA) (10 mM, pH 4.0) was added to the FITC labelled BUDAP@PSi-HA to

convert its surface charge from negative to positive, and the adhesion experiment was performed using uncoated-, mucin-coated, and transferrin-coated chamber slides/plates as described above.

4.20. DSS-induced colitis model

Male C57BL/6 mice (6-8 weeks) were purchased from Beijing Vital River Laboratory Animal Technology Co., Ltd. Mice were fed formulated drinking water containing 3% DSS (MW 36-50 kDa; MP Biochemical, Hlkirch, France) ad libitum throughout the experiment (day 0 to day 14). The body weights of mice were monitored and the weights were recorded as percentage of initial bodyweight. Clinical evaluations including the assessment of stool consistency and the detection of rectal bleeding were conducted to generate a modified disease activity index (DAI) score. Briefly, each parameter was scored on a scale from 0 to 9 and given a grade from 0 to 4 and then assessed as follows: (1) Stool consistency (0, well-formed dry pellets; 1, soft pellets; 2, loose wet stools; 3, diarrhea; 4,massive watery stool at crissum); (2) Fecal blood was tested with urine fecal occult blood test kit (Nanjing Jiancheng Bioengineering Institute, Nanjing China) (0, no color 2 min after adding the reagent; 1, the liquid gradually changed from light blue to blue within 30 s after adding the reagent; 2, the liquid was pale brown and gradually changed to clear blue-brown after adding the reagent within 10 s; 3, the liquid turn blue very quickly and a bit of blood was visible in the stool; 4, bloody stools, and the liquid turned into blue immediately; 5, the liquid was blue-brown immediately after adding the reagent and visibly bloody, with blood clotting on the anus and massive bleeding) [51].

4.21. In vivo adhesion experiments

Animals with colitis and normal controls were fasted overnight before experiments. For *in vivo* adhesion testing, each mouse received 100 μL Milli-Q water containing 2 mg PSi-Cy7/HA@LF or PSi-FITC/HA@LF by oral gavage. Milli-Q water rather than physiological

buffer solutions was used as vehicle due to the insolubility of LF in Milli-Q water. Animals were imaged at 2 and 5 h using IVIS Lumina II imaging system (PerkinElmer), and then immediately sacrificed after *in vivo* imaging. The colon was removed and imaged freshly after washing using IVIS Lumina II imaging system. The fluorescence signal intensity was quantified using Living Image software (PerkinElmer). For confocal imaging, the colon was washed with PBS for 3 times, and then embeds in tissue freezing medium for histologic section. Before confocal imaging, all the slices were stained by DAPI and F4/80 ab90247 to image the nucleus and macrophages, respectively.

4.22. In vivo treatment of established colitis

In vivo treatment experiments were performed using 10 groups: (1) disease-free control group (Normal), (2) colitis control group (Colitis), (3) free BUD, low dose (FBUDL), (4) free BUD, high dose (FBUDH), (5) AP@PSi-HA@LF particles, low dose (PL), (6) AP@PSi-HA@LF particles, high dose (PH), (7) BUD@PSi-HA@LF particles, low dose (BUDL), (8) BUD@PSi-HA@LF particles, high dose (BUDH), (9) BUDAP@PSi-HA@LF particles, low dose (BUDAPL), and (10) BUDAP@PSi-HA@LF particles, high dose (BUDAPH). Low dose and high dose were 0.5 mg/kg and 1.5 mg/kg BUD, respectively, or particles for the loading of 0.5 mg/kg and 1.5 mg/kg BUD, respectively. The vehicle for oral gavage was 100 μL Milli-Q water. Oral gavage was performed daily, after fasting the mice overnight, for 7 d. During the treatment period, body weight was recorded, and DAI was evaluated. After treatment, mice were sacrificed and the colon was collected. The colonic length was measured. Then, standard H&E-stained sections of colon were prepared, examined and scored. For cell infiltration of inflammatory cells, rare inflammatory cells in the lamina propria were counted as 0; increased numbers of inflammatory cells, including neutrophils in the lamina propria as 1; confluence of inflammatory cells, extending into the submucosa as 2; and a score of 3 was given for transmural extension of the inflammatory cell infiltrate. For epithelial damage,

absence of mucosal damage was counted as 0, discrete focal lymphoepithelial lesions were counted as 1, mucosal erosion/ulceration was counted as 2, and a score of 3 was given for extensive mucosal damage and extension through deeper structures of the bowel wall. The two subscores were added and the combined histologic score ranged from 0 (no changes) to 6 (extensive cell infiltration and tissue damage) [5, 52, 53].

TUNEL assay was performed according to the manufacturer's instruction, using the DeadEndTM TUNEL System Kit (G3250, Promega, Wisconsin, USA).

The blood samples were collected within orbital plexus, and centrifuged at 3000 rpm at 4 °C for 10 min to obtain serum. Blood serum sample was used to measure the levels of IL-1β and IL-6 with commercial ELISA kits.

All animal experiments were approved by the Animal Care and Use Committee of Xiamen University (China), and all protocols of animal studies conformed to the Guide for the Care and Use of Laboratory Animals.

4.23. Statistical analysis

All results were expressed as mean ± standard deviation (SD). A one-way analysis of variance (ANOVA) followed by the Bonferroni post hoc test was employed to analyze the data. The analysis was performed using OriginPro 9.0.0 software (OriginLab Corporation, USA) and the level of significance was set at the probabilities of $*p < 0.05$, $**p < 0.01$ and $***p < 0.001$.

Acknowledgements

W.L. acknowledges the Orion Research Foundation for financial support. T.B.-R. acknowledges financial support from the Fundação para a Ciência e a Tecnologia (grant no. SFRH/BD/110859/2015). H.Z. acknowledges Jane and Aatos Erkko Foundation (grant no. 4704010), Academic of Finland (grant no. 297580) and Sigrid Juselius Foundation (grant no. 28001830K1) for financial support. D.L. acknowledges the Jane and Aatos Erkko Foundation

for financial support. X.D. acknowledges financial support from the National Key R&D Program (Grant Nos. 2017YFA0504504 and 2016YFA0502001), the National Natural Science Foundation of China (Grant Nos. U1405223 and 81661138005), the Fundamental Research Funds for the Central Universities of China (Grant No. 20720160064), and the Program of Introducing Talents of Discipline to Universities (111 Project, B12001). H.A.S. acknowledges financial support from the Sigrid Juselius Foundation (Decision No. 4704580), the European Research Council under the European Union's Seventh Framework Programme (FP/2007-2013, Grant No. 310892) and the HiLIFE Research Funds.

Competing interests statement

The authors declare no competing interests.

Appendix A. Supplementary data

Supplementary data related to this article can be found at

References

[1] Kaplan GG. The global burden of IBD: from 2015 to 2025. Nat Rev Gastroenterol Hepatol. 2015;12:720-7.
[2] Lautenschläger C, Schmidt C, Fischer D, Stallmach A. Drug delivery strategies in the therapy of inflammatory bowel disease. Adv Drug Deliv Rev. 2014;71:58-76.
[3] Zhang S, Langer R, Traverso G. Nanoparticulate drug delivery systems targeting inflammation for treatment of inflammatory bowel disease. Nano Today. 2017;16:82-96.
[4] Herrera Estrada L, Wu H, Ling K, Zhang G, Sumagin R, Parkos CA, et al. Bioengineering bacterially derived immunomodulants: a therapeutic approach to inflammatory bowel disease. ACS Nano. 2017;11:9650-62.
[5] Zhang S, Ermann J, Succi MD, Zhou A, Hamilton MJ, Cao B, et al. An inflammation-targeting hydrogel for local drug delivery in inflammatory bowel disease. Sci Transl Med. 2015;7:300ra128.
[6] Date AA, Rais R, Babu T, Ortiz J, Kanvinde P, Thomas AG, et al. Local enema treatment to inhibit FOLH1/GCPII as a novel therapy for inflammatory bowel disease. J Control Release. 2017;263:132-8.
[7] Wilson DS, Dalmasso G, Wang L, Sitaraman SV, Merlin D, Murthy N. Orally delivered thioketal nanoparticles loaded with TNF-α–siRNA target inflammation and inhibit gene expression in the intestines. Nat Mater. 2010;9:923-8.

[8] Wang X, Yan J-J, Wang L, Pan D, Yang R, Xu Y, et al. Rational design of polyphenol-poloxamer nanovesicles for targeting inflammatory bowel disease therapy. Chem Mater. 2018;30:4073-80.
[9] Zhang Q, Tao H, Lin Y, Hu Y, An H, Zhang D, et al. A superoxide dismutase/catalase mimetic nanomedicine for targeted therapy of inflammatory bowel disease. Biomaterials. 2016;105:206-21.
[10] Ali H, Weigmann B, Neurath MF, Collnot EM, Windbergs M, Lehr CM. Budesonide loaded nanoparticles with pH-sensitive coating for improved mucosal targeting in mouse models of inflammatory bowel diseases. J Control Release. 2014;183:167-77.
[11] Huang Z, Gan J, Jia L, Guo G, Wang C, Zang Y, et al. An orally administrated nucleotide-delivery vehicle targeting colonic macrophages for the treatment of inflammatory bowel disease. Biomaterials. 2015;48:26-36.
[12] Lee CH, Lo LW, Mou CY, Yang CS. Synthesis and Characterization of Positive‐Charge Functionalized Mesoporous Silica Nanoparticles for Oral Drug Delivery of an Anti‐Inflammatory Drug. Adv Funct Mater. 2008;18:3283-92.
[13] Moulari B, Pertuit D, Pellequer Y, Lamprecht A. The targeting of surface modified silica nanoparticles to inflamed tissue in experimental colitis. Biomaterials. 2008;29:4554-60.
[14] Tirosh B, Khatib N, Barenholz Y, Nissan A, Rubinstein A. Transferrin as a luminal target for negatively charged liposomes in the inflamed colonic mucosa. Mol Pharm. 2009;6:1083-91.
[15] Serpe L, Canaparo R, Daperno M, Sostegni R, Martinasso G, Muntoni E, et al. Solid lipid nanoparticles as anti-inflammatory drug delivery system in a human inflammatory bowel disease whole-blood model. Eur J Pharm Sci. 2010;39:428-36.
[16] Knipe JM, Strong LE, Peppas NA. Enzyme- and pH-Responsive Microencapsulated Nanogels for Oral Delivery of siRNA to Induce TNF-α Knockdown in the Intestine. Biomacromolecules. 2016;17:788-97.
[17] Kang J, Joo J, Kwon EJ, Skalak M, Hussain S, She ZG, et al. Self-sealing porous silicon-calcium silicate core-shell nanoparticles for targeted siRNA delivery to the injured brain. Adv Mater. 2016;28:7962-9.
[18] Liu Z, Li Y, Li W, Xiao C, Liu D, Dong C, et al. Multifunctional nanohybrid based on porous silicon nanoparticles, gold nanoparticles, and acetalated dextran for liver regeneration and acute liver failure theranostics. Adv Mater. 2018;30:1703393.
[19] Turner CT, McInnes SJ, Melville E, Cowin AJ, Voelcker NH. Delivery of flightless I neutralizing antibody from porous silicon nanoparticles improves wound healing in diabetic mice. Adv Healthc Mater. 2017;6:201600707.
[20] Liu D, Bimbo LM, Mäkilä E, Villanova F, Kaasalainen M, Herranz B, et al. Co-delivery of a hydrophobic small molecule and a hydrophilic peptide by porous silicon nanoparticles. J Control Release. 2013;170:268-78.
[21] Wareing N, Szymanski K, Akkaraju GR, Loni A, Canham LT, Gonzalez-Rodriguez R, et al. In vitro gene delivery with large porous silicon nanoparticles fabricated using cost-effective, metal-assisted chemical etching. Small. 2017;13:1602739.
[22] Jinhwan K, Changshin J, Won‐Gwang L, Sungjin J, Mi LY, Jun L, et al. Programmed Nanoparticle‐Loaded Nanoparticles for Deep‐Penetrating 3D Cancer Therapy. Adv Mater. 2018:1707557.
[23] Li W, Liu D, Zhang H, Correia A, Makila E, Salonen J, et al. Microfluidic assembly of a nano-in-micro dual drug delivery platform composed of halloysite nanotubes and a pH-responsive polymer for colon cancer therapy. Acta Biomater. 2017;48:238-46.
[24] Li W, Liu Z, Fontana F, Ding Y, Liu D, Hirvonen JT, et al. Tailoring porous silicon for biomedical applications: from drug delivery to cancer immunotherapy. Adv Mater. 2018;30:1703740.

[25] Tang F, Li L, Chen D. Mesoporous Silica Nanoparticles: Synthesis, Biocompatibility and Drug Delivery. Adv Mater. 2012;24:1504-34.
[26] Lvov Y, Wang W, Zhang L, Fakhrullin R. Halloysite Clay Nanotubes for Loading and Sustained Release of Functional Compounds. Adv Mater. 2016;28:1227-50.
[27] Zhang H, Liu D, Shahbazi M-A, Makila E, Herranz-Blanco B, Salonen J, et al. Fabrication of a multifunctional nano-in-micro drug delivery platform by microfluidic templated encapsulation of porous silicon in polymer matrix. Adv Mater. 2014;26:4497-503.
[28] Shrestha N, Shahbazi M-A, Araújo F, Mäkilä E, Raula J, Kauppinen EI, et al. Multistage pH-responsive mucoadhesive nanocarriers prepared by aerosol flow reactor technology: A controlled dual protein-drug delivery system. Biomaterials. 2015;68:9-20.
[29] Gajanayake T, Olariu R, Leclère FM, Dhayani A, Yang Z, Bongoni AK, et al. A single localized dose of enzyme-responsive hydrogel improves long-term survival of a vascularized composite allograft. Sci Transl Med. 2014;6:249ra110.
[30] Joshi N, Yan J, Levy S, Bhagchandani S, Slaughter KV, Sherman NE, et al. Towards an arthritis flare-responsive drug delivery system. Nat Commun. 2018;9:1275.
[31] Wiener E, Levanon D. Macrophage cultures: an extracellular esterase. Science. 1968;159:217-.
[32] Sorokin L. The impact of the extracellular matrix on inflammation. Nat Rev Immunol. 2010;10:712-23.
[33] Wahl LM, Wahl SM, Mergenhagen SE, Martin GR. Collagenase production by endotoxin-activated macrophages. Proc Natl Acad Sci USA. 1974;71:3598-601.
[34] Ray P, Van Arsdall MR. Elevated Lipase during Initial Presentation of Ulcerative Colitis in a Pediatric Patient: Do We Check for It. Case Rep Gastroenterol. 2016;10:568-73.
[35] Vemula PK, Boilard E, Syed A, Campbell NR, Muluneh M, Weitz DA, et al. On-demand drug delivery from self-assembled nanofibrous gels: A new approach for treatment of proteolytic disease. J Biomed Mater Res A. 2011;97A:103-10.
[36] Strugala V, Dettmar PW, Pearson JP. Thickness and continuity of the adherent colonic mucus barrier in active and quiescent ulcerative colitis and Crohn's disease. Int J Clin Pract. 2008;62:762-9.
[37] Peterson CGB, Eklund E, Taha Y, Raab Y, Carlson M. A new method for the quantification of neutrophil and eosinophil cationic proteins in feces: establishment of normal levels and clinical application in patients with inflammatory bowel disease. Am J Gastroenterol. 2002;97:1755-62.
[38] Canny G, Levy O, Furuta GT, Narravula-Alipati S, Sisson RB, Serhan CN, et al. Lipid mediator-induced expression of bactericidal/ permeability-increasing protein (BPI) in human mucosal epithelia. Proc Natl Acad Sci USA. 2002;99:3902-7.
[39] Jubeh TT, Barenholz Y, Rubinstein A. Differential adhesion of normal and inflamed rat colonic mucosa by charged liposomes. Pharm Res. 2004;21:447-53.
[40] Liu D, Zhang H, Fontana F, Hirvonen JT, Santos HA. Microfluidic-assisted fabrication of carriers for controlled drug delivery. Lab Chip. 2017;17:1856-83.
[41] Kerdsakundee N, Li W, Martins JP, Liu Z, Zhang F, Kemell M, et al. Multifunctional nanotube-mucoadhesive poly(methyl vinyl ether-co-maleic acid)@hydroxypropyl methylcellulose acetate succinate composite for site-specific oral drug delivery. Adv Healthc Mater. 2017;6:1700629.
[42] McConnell EL, Basit AW, Murdan S. Measurements of rat and mouse gastrointestinal pH, fluid and lymphoid tissue, and implications for in-vivo experiments. J Pharm Pharmacol. 2008;60:63-70.
[43] Bimbo LM, Sarparanta M, Santos HA, Airaksinen AJ, Makila E, Laaksonen T, et al. Biocompatibility of thermally hydrocarbonized porous silicon nanoparticles and their biodistribution in rats. ACS Nano. 2010;4:3023-32.

[44] Brunauer S, Emmett PH, Teller E. Adsorption of gases in multimolecular layers. J Am Chem Soc. 1938;60:309-19.
[45] Schneider A, Picart C, Senger B, Schaaf P, Voegel J-C, Frisch B. Layer-by-layer films from hyaluronan and amine-modified hyaluronan. Langmuir. 2007;23:2655-62.
[46] Bauleth-Ramos T, Shahbazi M-A, Liu D, Fontana F, Correia A, Figueiredo P, et al. Nutlin-3a and cytokine co-loaded spermine-modified acetalated dextran nanoparticles for cancer chemo-immunotherapy. Adv Funct Mater. 2017;27:1703303.
[47] Leonard F, Collnot E-M, Lehr C-M. A three-dimensional coculture of enterocytes, monocytes and dendritic cells to model inflamed intestinal mucosa in vitro. Mol Pharm. 2010;7:2103-19.
[48] Frontela-Saseta C, López-Nicolás R, González-Bermúdez CA, Martínez-Graciá C, Ros-Berruezo G. Anti-inflammatory properties of fruit juices enriched with pine bark extract in an in vitro model of inflamed human intestinal epithelium: The effect of gastrointestinal digestion. Food Chem Toxicol. 2013;53:94-9.
[49] Butler M, Ng C-Y, van Heel DA, Lombardi G, Lechler R, Playford RJ, et al. Modulation of dendritic cell phenotype and functionin an in vitro model of the intestinal epithelium. Eur J Immunol. 2006;36:864-74.
[50] Leonard F, Ali H, Collnot E-M, Crielaard BJ, Lammers T, Storm G, et al. Screening of budesonide nanoformulations for treatment of inflammatory bowel disease in an inflamed 3D cell-culture model. ALTEX. 2012;29:275.
[51] Fan F, He Z, Kong L-L, Chen Q, Yuan Q, Zhang S, et al. Pharmacological targeting of kinases MST1 and MST2 augments tissue repair and regeneration. Sci Transl Med. 2016;8:352ra108.
[52] Dieleman, Palmen, Akol, Bloemena, PeÑA, Meuwissen, et al. Chronic experimental colitis induced by dextran sulphate sodium (DSS) is characterized by Th1 and Th2 cytokines. Clin Exp Immunol. 1998;114:385-91.
[53] Siegmund B, Rieder F, Albrich S, Wolf K, Bidlingmaier C, Firestein GS, et al. Adenosine kinase inhibitor GP515 improves experimental colitis in mice. J Pharmacol Exp Ther. 2001;296:99.

Graphical abstract

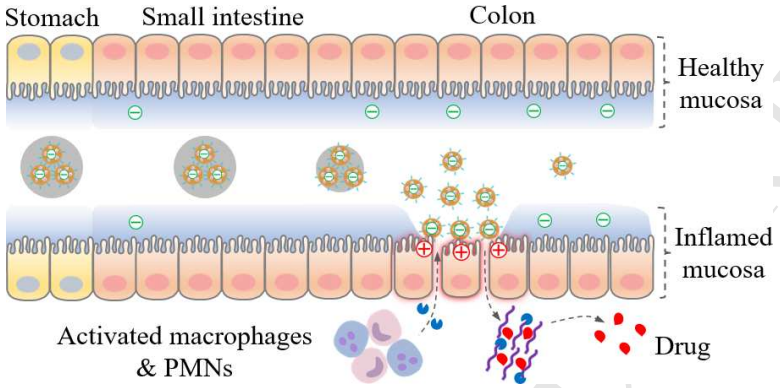

(Graphical abstract)